

Study on the Aerodynamic Characteristics of Unmanned Aerial Vehicles

Amarmend GALSANDORJ^a, Uyanga SUKHBAATAR^{*b}, Daariimaa ENKHTUYAU^c
Nomungerel ERDENEBAT^d

^{a,b,c,d}*Department of Transportation, School of Mechanical Engineering and Transportation,
Mongolian University of Science and Technology, Mongolia*

^a*E-mail : amarmend@must.edu.mn*

^b*E-mail : uyanga@must.edu.mn*

^c*E-mail : daariimaa@must.edu.mn*

^d*E-mail : nomungerel@gmail.com*

Abstract: This study investigates the optimization of engine placement on the wing to enhance lift force and aerodynamic efficiency without increasing engine power or wing surface area. Experiments were conducted in a controlled laboratory environment using an open-circuit wind tunnel with airflow velocities ranging from 25.2 to 35.2 m/s. Lift force generation was analyzed by positioning the propeller at -2 mm, 0.5 mm, 10 mm, and 12 mm along the Y-axis relative to the wing's leading edge. Results indicate that positioning the engine 10 mm above the leading edge increases the airflow velocity over the upper wing surface, leading to a reduction in pressure and an increase in lift force. This configuration enhances aerodynamic performance and enables greater payload capacity without additional power input.

Keywords: wings, lift, electric motor and propeller

1. INTRODUCTION

In recent years, numerous countries have conducted research on the integration of one or more electric motors in unmanned aerial vehicles (UAVs), considering their geographic and operational environments [1]. The implementation of multiple electric motors aims to enhance aerodynamic performance by optimizing their placement and interaction with other aerodynamic surfaces. NASA, in the United States, has developed the **X-57 Maxwell**, a multi-engine electric aircraft featuring a five-blade propeller and a high-aspect-ratio wing with distributed electric propulsion. Studies on this aircraft have examined its aerodynamic characteristics, particularly the lift distribution along the X and Z axes.

The lift force on an aircraft depends on several factors, including the speed of the aircraft. It has been theoretically proven that placing an air propeller in front of the wing can increase the air speed on the wing and enhance the lift force.

As the angle of attack of the wing increases, the laminar flow over the upper surface of the wing may separate and turn into a turbulent flow, resulting in reduced airspeed over the wing and decreased lift. However, by placing a propeller on the leading edge of the wing, it is possible to increase the angle of attack and lift, as well as improve the lift-to-drag ratio, by directing the turbulent flow towards the upper surface of the wing. These concepts have been supported by theoretical research and some studies.

According to Bernoulli's principle, an increase in the velocity of a fluid occurs simultaneously with a decrease in static pressure. When the propeller is mounted at the leading edge of the wing, it accelerates airflow over the upper surface of the airfoil. As a result, the pressure above the wing decreases relative to the pressure below it, creating a net upward force known as lift. This phenomenon is described by Bernoulli's equation:

$$P + \frac{1}{2}\rho V^2 + \rho gh = \text{constant} \quad (1)$$

where P is static pressure, ρ is air density, V is air velocity, and h is elevation.

The increased velocity over the upper surface due to the propeller's slipstream enhances this pressure differential, thereby increasing the overall lift. This effect becomes more pronounced when the engine is positioned optimally (e.g., 10 mm above the wing's leading edge), as the airflow attachment and distribution are improved, delaying flow separation and increasing the effective angle of attack.

2. MAIN SECTION

The aerodynamic benefit of placing a propeller near the wing is a well-established concept, this study contributes new insight by experimentally identifying the optimal vertical placement of a propeller (10 mm above the leading edge) specifically for small-scale UAV configurations. Unlike many previous studies that rely solely on numerical simulations or large-scale aircraft analysis, this research integrates both wind tunnel experimentation and CFD simulation to validate findings on a compact platform. This combined methodology provides practical value for the design of lightweight UAVs where precision airflow control is critical

The propeller and wing profile have some basic geometric parameters, and Figure 1 illustrates the distance between the propeller and the wing along the Z and Y axes. For the wing console used in the study, the length was 2.2 m and the average aerodynamic chord of the profile was 0.42 m. The length of the root part was 0.49 m, and the length of the tip was 0.35 m.

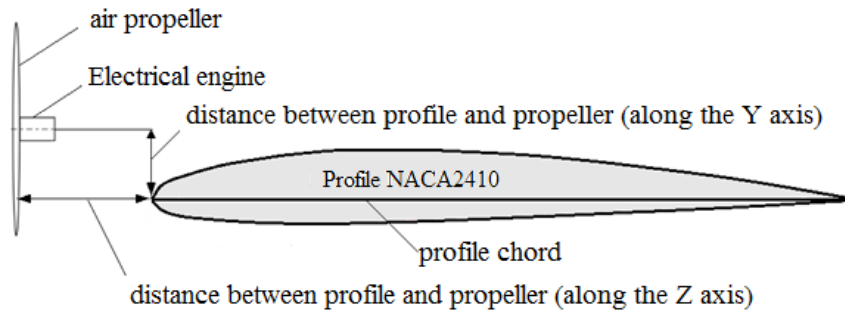


Figure. 1. Basic geometrical parameters of the propeller and profile

A propeller is a bladed aerodynamic device that operates in an air medium, driven by an engine, and functions as a propulsion unit that converts engine power (torque) into thrust. As illustrated in Figure 2, the central section of the propeller generates the highest dynamic pressure, accelerating the airflow beyond its initial velocity as it passes through the propeller.

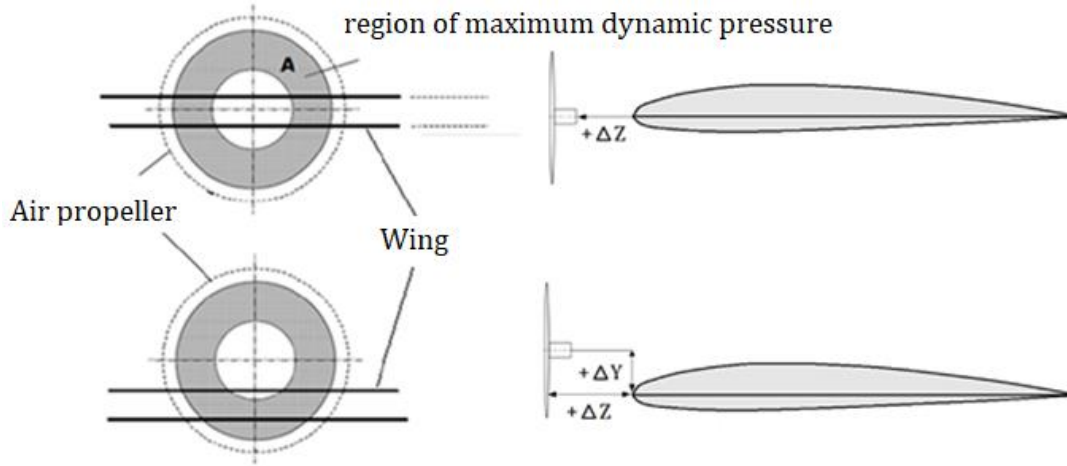


Figure. 2. Relations between the propeller and the wing

The increase in lift is made possible by the increased air speed on the wing and corresponding decrease in pressure. As part of the study, researchers investigated the potential for increased lift by placing a zone of high dynamic propeller pressure on the upper surface of the wing. They accomplished this by testing the engine position Z_p , $X_p = \text{const}$ at different distances above the leading edge of the wing profile along the Y_p axis. Specifically, they tested the position of the engine at distances of -2 mm, 0 mm, 5 mm, 10 mm, and 12 mm. In order to determine the lift of the wing, the researchers tested the position of the engine by placing it in five different positions above the leading edge of the wing, as shown in Figure 3.

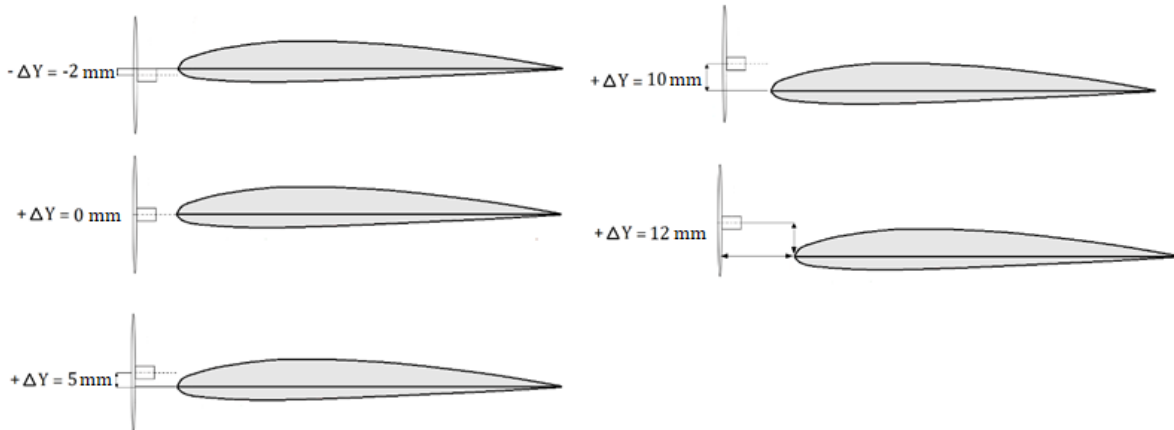


Figure. 3. The engine mount was positioned at five different distances above the leading edge of the wing: 2mm, 0mm, 5mm, 10mm, and 12mm

While the aerodynamic benefit of increasing lift by blowing air over the upper surface of a wing is well known, the key novelty of this study lies in experimentally and numerically comparing multiple propeller positions (-2 mm, 0 mm, 5 mm, 10 mm, and 12 mm) to determine the most effective configuration for small unmanned aerial vehicles (UAVs). Unlike previous studies that focused on theoretical modeling or large-scale aircraft simulations, this work demonstrates a validated optimization approach specifically tailored to lightweight UAVs based on both experimental and computational evidence.

3. EXPERIMENT

The study involved the installation of four electric motors on the leading edge of a wing with a length of 0.785 m and a profile of 0.165 m (Figure 4). These dimensions were 2.8 times smaller than the calculated values. The wing was tested in an open wind tunnel, and the angle of attack was varied between 0 and 16 degrees during the experiment.



Figure 4. The electric motor was located on the leading edge of the wing



Figure 5. A smoke test was conducted in the wind tunnel to observe the behavior of the electric motor.

To determine the lift force generated by the propellers at various points on the leading edge of the wing, an experiment was conducted in an open wind tunnel at a speed ranging from 25 to 35.2 m/s. Thin wires were placed at two locations on the upper surface of the wing (Figure 5) to investigate the turbulent flow resulting from changes in the angle of attack. The study also involved a comparison of turbulent flow with and without the propeller.

The lift force generated by the wing is determined by several factors, including the speed, height, and area of the airflow flowing over the wing. The study focuses on how the lift force changes as the air speed increases due to the installation of more propellers on the wing. The lift force of the wing can be calculated using Equation (2).

$$Y = C_y \cdot \frac{\rho \cdot V^2}{2} \cdot S \quad (2)$$

where: C_y - lift coefficient, ρ - air density (depending on aircraft height), V - aircraft speed (m/s), S - wing area (m^2).

The experiment held constant the air density and wing area, but varied the flight speed and lift in order to measure the effect of installing multiple propellers on the wing.

In this study, the air density and wing area were kept constant. The airflow velocity (V) was varied by changing wind tunnel speed and propeller location. However, the lift coefficient (C_l)—which depends on the angle of attack, flow attachment, and boundary layer behavior—was not directly analyzed.

A more detailed examination of C_l , either through CFD data or empirical measurements, could clarify how propeller position influences aerodynamic efficiency. Understanding how C_l changes with engine placement would also support the physical reasoning behind the observed increase in lift.

The experiment held constant the air density and wing area, but varied the flight speed and lift in order to measure the effect of installing multiple propellers on the wing.

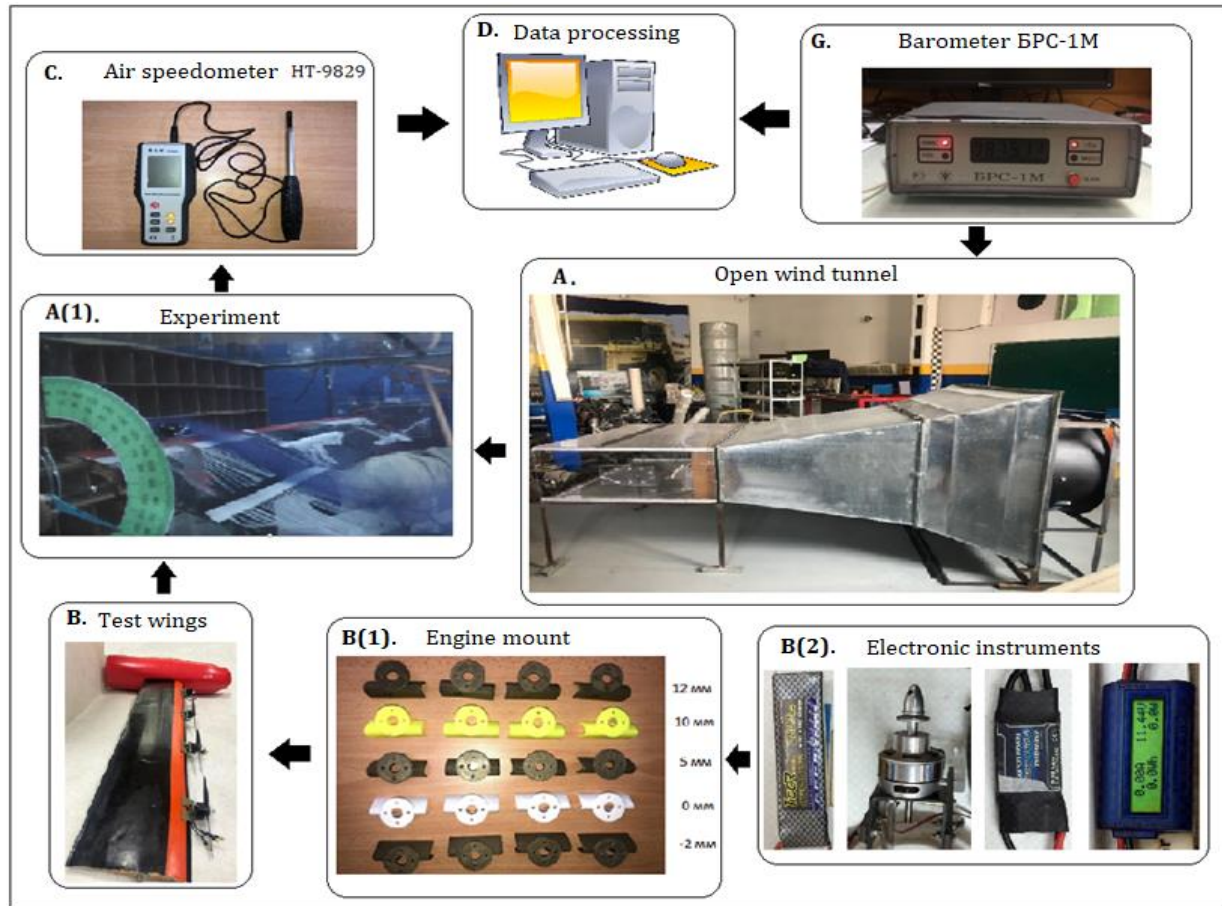


Figure 6. Wind tunnel testing process. Figure 11 illustrates the pressure coefficient (C_p) and the X-direction velocity (V_x) from the CFD simulation. The C_p plot shows a significant reduction in pressure above the wing in the region influenced by the propeller slipstream, which corresponds to the increased lift. Simultaneously, the V_x plot indicates accelerated airflow reaching up to 35 m/s directly above the wing, where the propeller is located. This increased velocity over the upper surface results in a lower pressure zone, in accordance with Bernoulli's principle, confirming the aerodynamic advantage of the 10 mm propeller offset configuration.

Atmospheric pressure was measured using a BRS-1M barometer (G) to account for its effect on the lift determination in a wind tunnel (A). The airspeed over the wing surface and the wind tunnel were measured using an HT-9829 (C) speedometer and used in the experimental calculations. The test object, equipped with four electric motors on the leading edge of the wing (B, B(1), B(2)), was placed inside the wind tunnel (A(1)), and the air flow was blown at a speed of 25.2-35.2 m/s. The lift was calculated using a NACA 2410 airfoil wing and an engine mount with -2mm, 0mm, 5mm, 10mm, 12mm lift in the Y-axis above the leading edge of the wing.

4. A SIMULATION EXPERIMENT

Chinese scientists Weijia Fu, Jie Li and Haojie Wang conducted experiments on modeling a flying wing with an air engine. Scientists Giulia Chirico and George N. Baracos also performed experiments to simulate the direction of rotation of a transport aircraft propeller. The simulation I did differed from them in that it determined the optimal position of the engine along the Y axis in a small drone. Simulation results were obtained using the ANSYS Fluent program to determine the lift force of a four-rotor wing.

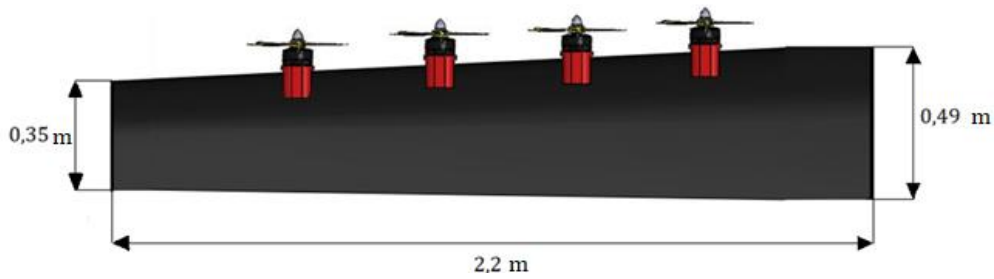


Figure 7. Model used in modeling Ansys Fluent

The simulation has been modified to change the airflow speed from 25.2 m/s to 35.2 m/s and the propeller speed to 3500 rpm. Simulation conditions and wing dimensions are given in Table 1 below.

Table 1. Wing parameters used in the ANSYS Fluent test

№	Characteristics	
1	Profile type	NACA 2410
2	Reynolds number	$0.874 \cdot 10^6$
3	Air density	1.0413 kg/m^3
4	Viscosity of air (18°C)	$1.8 \cdot 10^{-5} \text{ kg/(m}\cdot\text{sec)}$
5	Mean aerodynamic chord	0.42 m
6	Console length	2.2 m
7	Root chord	0.49 m
8	tip chord	0.35 m

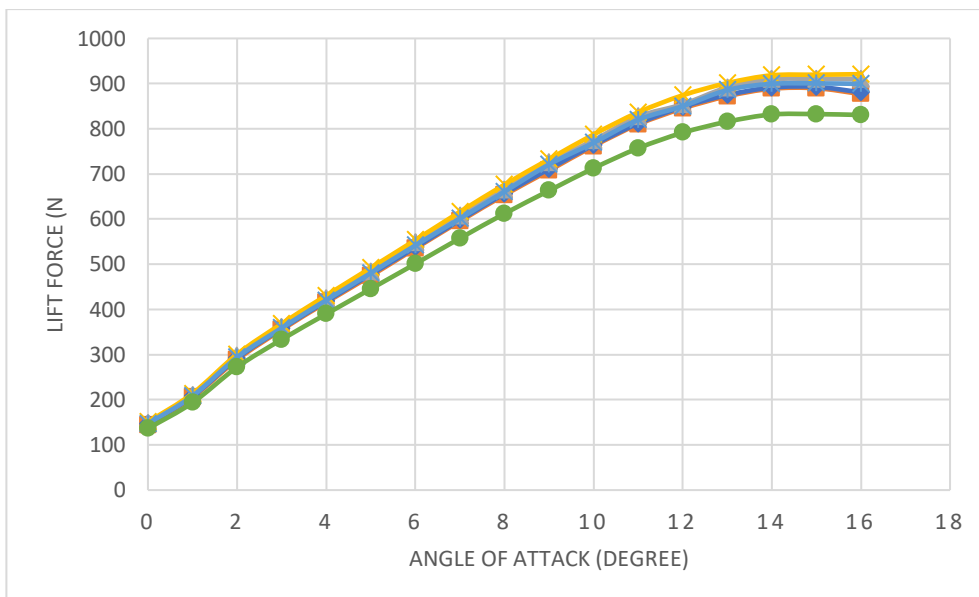


Figure 8. A comparative graph showing how the lift force of the wing changes as the position of the engine is varied:


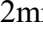
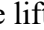
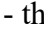
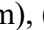
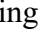
() - the lift force when the engine is positioned 2mm below the leading edge of the wing (Y= -2mm), () - The engine is positioned at the leading edge of the wing (Y=0 mm), () - The lift force when the engine is located 5mm above the leading edge of the wing (Y= 5mm), () - the lift force when the engine is positioned 10mm above the leading edge of the wing (Y=10mm), () - The lift force when the engine is positioned 10mm above the leading edge of the wing (Y=1mm), () - the lift force generated by the wing when the engine is mounted at a location other than the leading edge

Table 2. Calculation of engine-based and non-engine wing lift at the front edge of the wing

	The engine is positioned 10 mm above the front edge of the wing			Engine isn't installed at the front edge of the wing.			
Angle of attack (degree)	Tandem rear wing (N)	Tandem front wing (N)	Total (N)	Tandem rear wing (N)	Tandem front wing (N)	Total (N)	Growth rate (%)
0	150,5	149,5	300.06	136.21	132.22	268.44	11.778127
1	213,8	212,4	426.24	193.49	187.82	381.31	11.781304
2	300,7	298,8	599.57	272.2	264.229	536.431	11.770074
3	368,3	365,9	734.29	333.33	323.574	656.912	11.779051
4	430,7	427,9	858.69	389.8	378.389	768.196	11.780066
5	492	488,9	980.98	445.35	432.309	877.663	11.77183
6	553,5	550,04	1103.5	500.95	486.284	987.242	11.78009
7	615,9	612,0	1227.9	557.42	541.099	1098.52	11.780695
8	676,2	672,01	1348.2	612.05	594.124	1206.17	11.775561
9	732,4	727,8	1460.2	662.87	643.457	1306.33	11.780245
10	787,3	782,4	1569.7	712.6	691.728	1404.32	11.776513
11	836,3	831,1	1667.4	756.91	734.741	1491.65	11.780018
12	874,1	868,7	1742.8	791.19	768.021	1559.22	11.77462
13	901,1	898,5	1796.6	815.62	791.737	1607.36	11.775483
14	918,3	912,62	1830.9	831.62	806.83	1638	11.7459

The most valuable of the three test results was the identification of the 10mm lift motor position, which increased the lift generated by the propeller on the wing. To measure the wing lift force, we varied the angle of attack of the wind tunnel from 0 to 16 degrees.

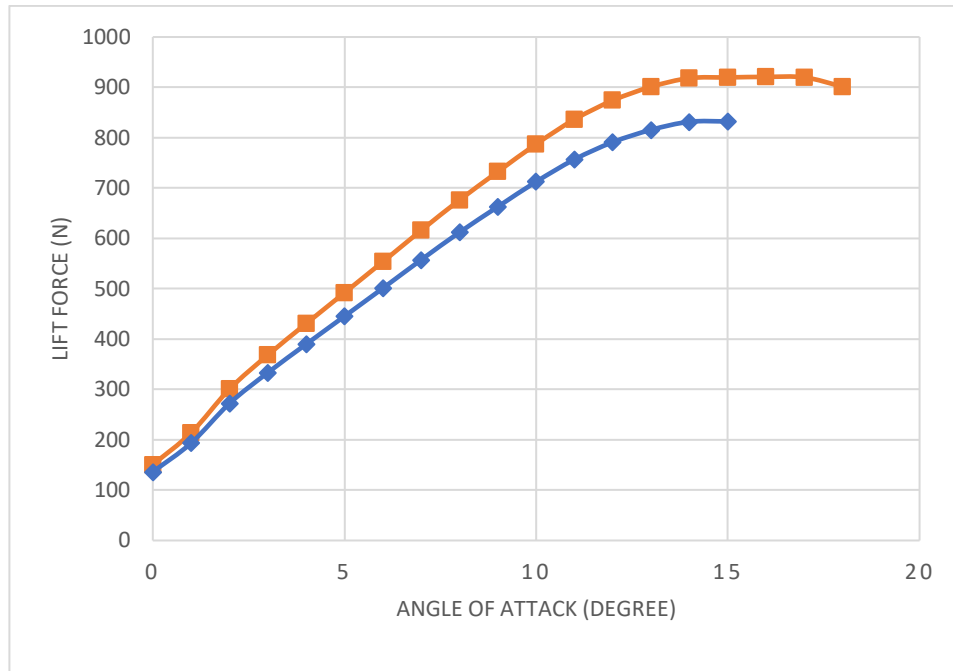


Figure 9. Wing lifting force comparison graph
 (—■—) – lifting force when the engine is at a height of 10 mm from the leading edge of the wing ($Y=10$ mm), (—◆—) – lifting force when the engine is not mounted on the leading edge of the wing

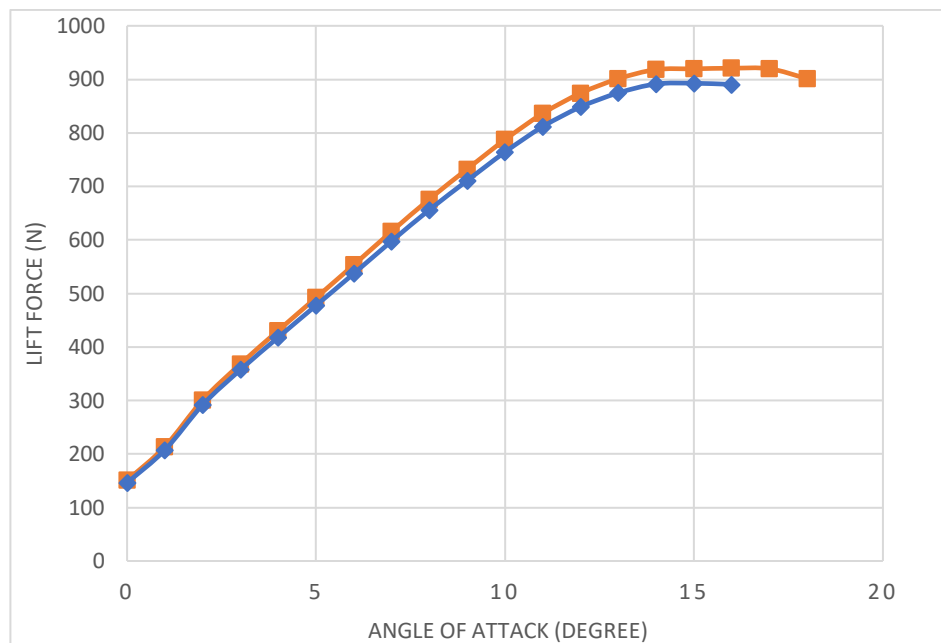


Figure 10. Wing lifting force comparison graph
 (—■—) – lifting force when the engine is at a height of 10 mm from the leading edge of the wing ($Y=10$ mm), (—◆—) – the engine is located on the leading edge of the wing ($Y=0$ mm)

In Figure 9, the engine is situated 10 mm above the wing's leading edge and not mounted on it. This positioning indicates that the maximum angle of attack of the unpowered wing is 15 degrees, with lift decreasing as the angle of attack increases. However, with the engine mounted

10 mm above the leading edge, the maximum angle of attack increases to 16.3 degrees, a gain of 1.3 degrees. As shown on the figure, the lift increases with each adjustment in the wing's angle of attack when the engine is raised 10mm above the leading edge. Figure 10 displays two engines' placement with a symmetrical electric motor fixed on the wing's leading edge, also 10 mm above the leading edge.

The calculation of wing lift assumed a constant air density and wing area, while the lift coefficient was varied between 0 and 16 degrees of angle of attack at flight speeds of 25.2-35.2 m/s. Simulation testing was conducted by adjusting the speed, with the main factor affecting lift being the velocity difference between the upper and lower surfaces of the wing. ANSYS Fluent was used to calculate this difference, and the resulting value was compared to that obtained from the wind tunnel.

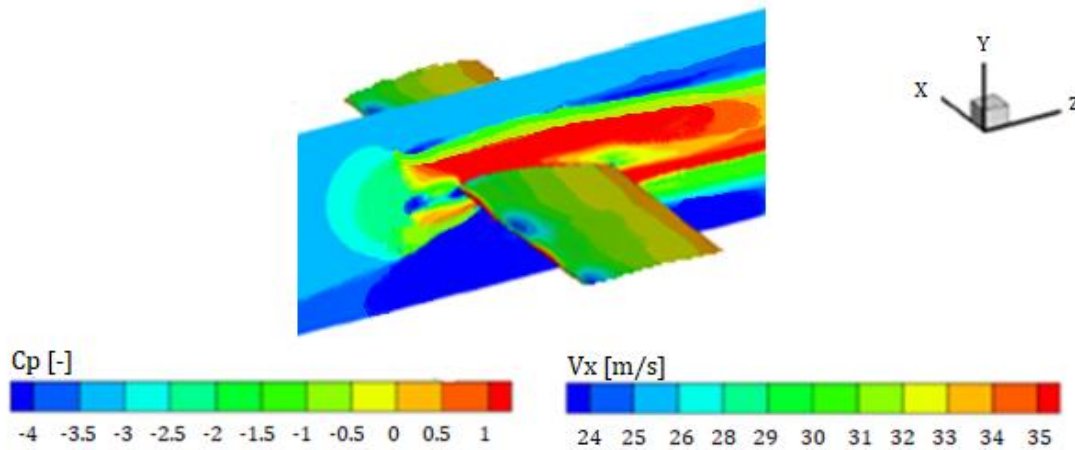


Figure 11. Change in airflow speed and pressure when the engine is at a height of 10 mm from the leading edge of the wing (simulation)

Figure 11 shows that the air flow on the wing surface increases where the propeller engine is located, as observed in the simulation. An increase in air flow on the wing surface can lead to an increase in lift. Figure 11 illustrates the pressure coefficient (C_p) and the X-direction velocity (V_x) from the CFD simulation. The C_p plot shows a significant reduction in pressure above the wing in the region influenced by the propeller slipstream, which corresponds to the increased lift. Simultaneously, the V_x plot indicates accelerated airflow reaching up to 35 m/s directly above the wing, where the propeller is located. This increased velocity over the upper surface results in a lower pressure zone, in accordance with Bernoulli's principle, confirming the aerodynamic advantage of the 10 mm propeller offset configuration.

To better understand the aerodynamic behavior influencing lift generation, additional post-processing of the simulation results was performed. The pressure distribution over the wing surface was visualized using contour plots, revealing a significant decrease in pressure along the upper surface when the engine is positioned 10 mm above the leading edge. This pressure drop correlates with increased local airflow velocity, as confirmed by velocity vector fields and streamline analysis.

The streamline patterns indicate accelerated and more attached flow over the wing at higher angles of attack, with delayed flow separation compared to cases where the engine is mounted on or below the leading edge. These findings support the hypothesis that propeller-induced slipstream alters the boundary layer behavior and enhances lift generation through increased dynamic pressure and better flow attachment.

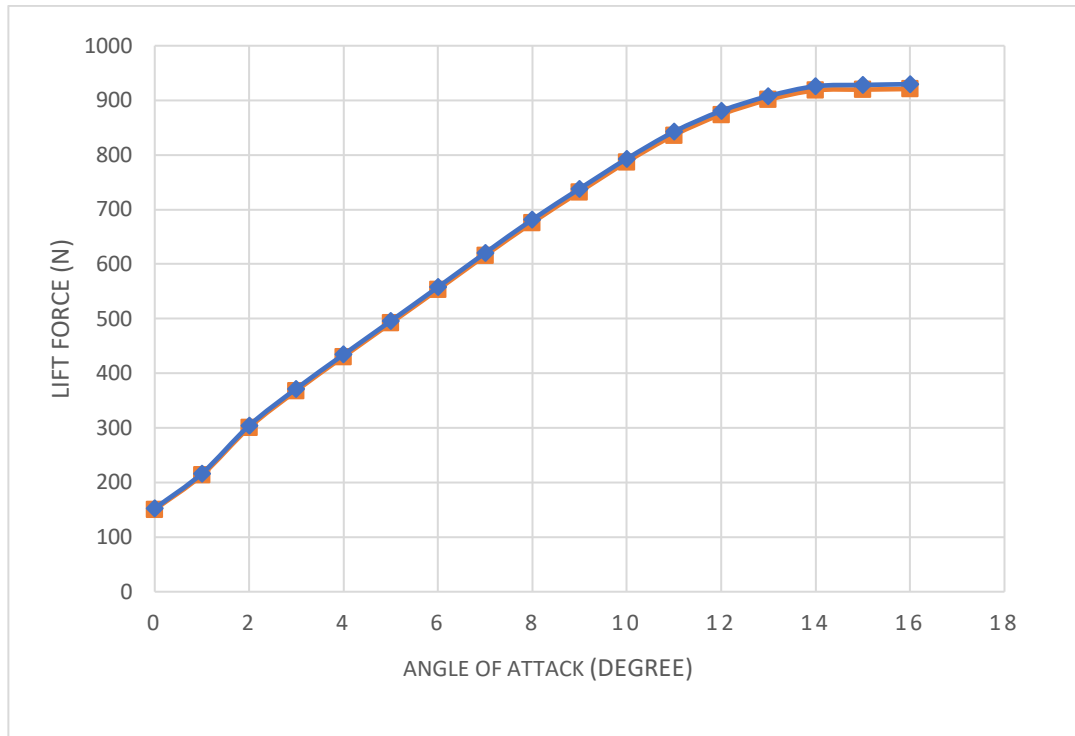


Figure 12. Comparative graph of simulation and experiment

(—■—) experiment - lifting force when the engine is at a height of 10 mm from the leading edge of the wing, (—◆—) simulation - lift when the engine is at a height of 10 mm from the leading edge of the wing

Based on the experiments and simulation data, the simulation results showed a higher lift of 2.1-8.5 N, depending on the angle of attack (Fig. 10). It was concluded that the simulated lift was 0.21-0.88 kg, depending on the angle of attack, due to the inability to accurately measure the airflow velocity over the wing, which was an experimental value obtained in the wind tunnel.

While both experimental and simulation results demonstrate the positive effect of engine placement on lift, the simulation yielded higher lift values—ranging from 2.1 N to 8.5 N more than the physical tests. This discrepancy can be attributed to several factors. First, CFD simulations are based on idealized assumptions such as uniform airflow, perfect geometry, and no mechanical vibration or thermal distortion. In contrast, real-world wind tunnel testing includes physical imperfections such as turbulence at the inlet, sensor inaccuracy, and limitations in model scale or motor control.

Additionally, precise measurement of airflow velocity over the wing was limited in the experiment, whereas in ANSYS Fluent, the velocity field was computed directly at high resolution. These factors collectively explain why simulated lift exceeds experimental results. Despite the discrepancy, the trends in both results confirm that a propeller positioned 10 mm above the leading edge significantly improves lift, validating the overall design hypothesis.

5. DISCUSSION

This study focused on optimizing the vertical placement of a propeller to improve lift in small UAV configurations. Compared to Shurouq et al. [4], who enhanced performance using a tandem-wing design, our approach retains a single-wing layout and achieves lift enhancement through targeted propulsion placement. While tandem configurations increase surface area and stability, our method is structurally simpler and more adaptable.

Alba et al. [3,14] used a surrogate-based optimization framework for wing-propeller interaction, focusing on multi-objective design improvements. In contrast, our approach is experimentally grounded and directly targets lift performance, offering practical insight for lightweight UAVs without relying on complex simulations.

Weijia Fu et al. [16] numerically analyzed slipstream effects, confirming increased lift through propeller-induced airflow. Our study expands on this by validating the effect experimentally and determining the most effective engine position, adding practical applicability.

Overall, this research bridges theoretical, computational, and empirical methods by identifying an optimal engine position (10 mm above the leading edge) to significantly improve lift without altering wing geometry or increasing power input.

The current simulation was limited to a single geometric configuration and primarily focused on lift force. While the results confirm the effect of engine position on lift, important aerodynamic aspects such as drag, turbulence, and wake swirl were not analyzed. Including these factors in future simulations would provide a more complete understanding of propeller-wing interaction, particularly for evaluating efficiency, stability, and real-world performance. Extending the simulation to assess drag-to-lift ratio and flow unsteadiness would strengthen the aerodynamic conclusions.

CONCLUSION

The effect of propeller position on wing lift was experimentally studied by mounting the engine on the leading edge of the wing and varying its location along the Y-axis. The results showed that the propeller can increase the airflow on the upper surface of the wing and boost lift. At an elevation angle of $Y = 10$ mm, the lift force of the wing is 12.08 N at an angle of attack of zero degrees, and it increases to 69.14 N at an angle of attack of 15 degrees.

The engine is mounted 10mm above the leading edge of the wing, the maximum angle of attack is 16.3 degrees, increasing by 1.3 degrees.

LITERATURE

G. Ameyugo, M. Taylor, and R. Singh, Distributed Propulsion Feasibility Studies, 25th International Congress of the Aeronautical Sciences (2006).

Giulia Chirico, George N. Barakos, Nicholas Bown 2018. Propeller installation effects on turboprop aircraft acoustics.

Christian Alba 2018. A Surrogate-based multi-disciplinary design optimization frameworks modeling wing-propeller interaction

Omar Abdulrazzak Khudair Shurouq Adnan Aziz Huda Ail Munshid Haedar Muhey Rzokhy Samiah Fared 2016. Improvement of Micro UAV Performance using Tandem-Wing Design

Tomas Sinnige 2018. Aerodynamic Analysis of Interaction Effects and Comparison with Conventional Layout.

Турманидзе Р.С. Повышение летно-технических характеристик летательных аппаратов путем применения винта изменяемой геометрии / Р.С. Турманидзе, Л. Дадоне, Г.О. Санадзе. // Труды 5-го форума Российского вертолетного общества. – М.: МАИ. – 2002.

Abbott, I. H., and von Doenhoff, A., Theory of Wing Sections, McGraw–Hill, New York, 1959, Chap. 5.

D. P. Witkowski, A. K. H. Lee, and J. P. Sullivan, Aerodynamic Interaction between Propellers and Wings, Journal of Aircraft **26**, 829 (1989).

L. Prandtl, Mutual Influence of Wings and Propeller, The First Report of the Goettingen Aerodynamic Laboratory, Chapter 4, Section 6 (1921).

L. L. M. Veldhuis and P. M. Heyma, Aerodynamic optimisation of wings in multi-engined tractor propeller arrangements, Aircraft Design **3**, 129 (2000).

L. L. M. Veldhuis, Review of Propeller-Wing Aerodynamic Interference, 24th International Congress of the Aeronautical Sciences (2004).

R. H. Stone, Aerodynamic Modeling of the Wing-Propeller Interaction for a Tail-Sitter Unmanned Air Vehicle, Journal of Aircraft **45**, 198 (2008).

Michael D. Patterson 2016. Conceptual design of high-lift propeller systems for small electric aircraft.

Maurice F. M. Hoogreef, Roelof Vos, and Reynard de Vries. Veldhuis Delft University of Technology, Faculty of Aerospace Engineering, Delft, The Netherlands 2019. Conceptual Assessment of Hybrid Electric Aircraft with Distributed Propulsion and Boosted Turbofans.

Christian Alba, Ali Elham, Brian J. German, Leo Veldhuis 2018. A surrogate-based Multi-Disciplinary Design optimization framework modeling wing-propeller interaction 2018.

I. Kroo, Propeller-Wing Integration for Minimum Induced Loss, Journal of Aircraft **23**, 561 (1986).

Weijia Fu, Jie Li, Haojie Wang. Numerical Simulation of Propeller Slipstream Effect on A Propeller-driven Unmanned Aerial Vehicle. Procedia Engineering **31** (2012) 150 – 155

Giulia Chirico, George N. Barakos, Nicholas Bown. Propeller installation effects on turboprop aircraft acoustics. Journal of Sound and Vibration **424** (2018) 238–262